International Journal of Advanced Engineering Research and Science (IJAERS)
Peer-Reviewed Journal
ISSN: 2349-6495(P) | 2456-1908(O)
Vol-12, Issue-6; Jun, 2025
Journal Home Page Available: https://ijaers.com/
Article DOI: https://dx.doi.org/10.22161/ijaers.126.4

Development of artificial aggregates by using sodium silicate activated copper tailings and slag

Demagh Lotfi[1], Hui Wang[2], Samuel Aires Master Lazaro[1], Lanping Qian[2], Xiangyu Li[2]

[1]College of Civil Engineering, Taiyuan University of Technology, Taiyuan, 030024, China
[2]Key Laboratory of Urban Security and Disaster Engineering of Ministry of Education, Beijing Key Laboratory of Earthquake Engineering and Structural Retrofit, Beijing University of Technology, Beijing 100024, China.

Received: 03 May 2025,
Receive in revised form: 04 Jun 2025,
Accepted: 09 Jun 2025,
Available online: 13 Jun 2025

***Keywords*— Granulation; Alkali activation, artificial aggregate, copper tailings, sodium silicate**

***Abstract*—** *This study investigated the development of artificial aggregates using copper tailings activated by sodium silicate via granulation. Five different mixes were prepared by incorporating varying amounts of ground granulated blast furnace slag (GGBS) and sodium silicate. The granulation process was performed in a rotating disk granulator, with water sprayed onto the dry mixture to facilitate binding. The resulting aggregates, ranging from 5 to 25 mm in diameter, were cured in a humid environment for 3, 7, and 28 d. The aggregates were then tested for size distribution, oven-dried density, water absorption, crushing strength, and individual-granule strength. Microstructural analysis was conducted using scanning electron microscopy (SEM) and X-ray computed tomography (XCT). The results showed that the addition of GGBS significantly improved the properties of the artificial aggregates, resulting in a higher density, lower water absorption, and increased strength.XCT images revealed a more refined pore structure with smaller and more evenly distributed pores in the GGBS-containing samples. The crushing strength and individual granule strength followed a Weibull distribution, with the GGBS samples exhibiting higher strength values. SEM analysis confirmed the formation of N-A-S-H gel in the GGBS samples, which acted as a binding phase and improved the microstructure. These findings demonstrate the potential of using copper tailings and GGBS to produce sustainable artificial aggregates with enhanced properties for construction applications.*

I. INTRODUCTION

Copper tailings, a substantial byproduct of copper mining, are a significant source of industrial waste, particularly in regions with high copper production, such as China. For every ton of copper produced, approximately 300 tons of tailings are generated, with provinces such as Jiangxi, Hubei, and Yunnan serving as key contributors to this waste stream [1,2].These tailings are primarily stored in dams or impoundments, posing critical environmental challenges because of their large volumes and potential for heavy metal leaching [1].Addressing these issues through the effective management and utilisation of copper tailings is imperative for mitigating environmental impacts and advancing sustainable industrial practices.

Simultaneously, the global demand for natural aggregates, such as sand, gravel, and crushed stone, continues to rise steadily, driven by rapid economic development and population growth. These aggregates play a vital role in construction, providing essential properties such as strength, durability, and stability to materials such as concrete, asphalt, and building foundations [3]. However, the growing demand has led to resource depletion, environmental degradation, and increased carbon footprints. Consequently, stricter regulations on natural

aggregate sourcing have created an urgent need to develop sustainable alternatives. Recycling industrial byproducts, such as copper tailings, into artificial aggregates offers a promising solution for waste management and the growing demand for construction materials [4].

The use of waste materials such as fly ash, blast furnace slag, red mud, steel slag, and recycled concrete to produce artificial aggregates has gained significant attention in research because of its potential to mitigate environmental impact and provide sustainable construction materials [5]. These materials, derived from industrial and construction waste streams, offer a promising solution for aggregate production using various methods, each with unique characteristics and benefits [6].

Research has revealed the compelling properties of various alternative aggregates in different construction applications. Fly ash aggregates serve as excellent thermal insulators [7] while significantly reducing the concrete structure weight by up to 30% compared to traditional options [8].Steel slag is known for its mechanical performance, with its high density and angular shape producing concrete that is 15-25% stronger in compression than conventional alternatives [9].Recycled concrete aggregates (RCA) have also shown promising results, achieving strength levels close to those of natural aggregates [10].Although they tend to absorb more water, this property can benefit internal curing processes [11]. Through careful mix design optimization, RCA concrete can reach 90-95% of conventional concrete's strength, demonstrating its viability as a sustainable alternative [12].

However, using waste materials for artificial aggregates faces issues with inconsistent material properties and quality control, making it difficult to achieve reliable structural performance [13].The processing and treatment requirements to remove contaminants and ensure safety add significant costs to production [5].Meeting strict construction standards and building codes remains challenging because of the variability in waste material composition [14]. Market acceptance is limited by concerns about long-term durability and environmental impact, despite the sustainability benefits [15, 16].

Granulation is the most effective method for producing artificial aggregates from copper tailings because of its ability to efficiently handle fine-grained materials through rolling and tumbling motions, creating irregular or quasi-spherical rather than perfect spherical granules with good mechanical properties [17], improving the strength and durability of the resulting aggregates for construction applications [18, 19].This process is particularly suitable for copper tailings because this material typically has an ideal particle size distribution and moisture content for granulation, and its fine particles readily bind together during rolling [20].This method requires minimal equipment compared with alternatives such as extrusion or pressing, making it cost-effective and easy to implement at mining sites. It also minimizes environmental impact through lower energy consumption and dust emission control.

Alkali activation offers another viable approach for recycling copper tailings into artificial aggregates. This method uses alkaline solutions, such as sodium hydroxide and sodium silicate, to chemically bind raw materials, such as copper tailings, into strong, durable aggregates [21].The properties of alkali-activated materials can be tailored by adjusting parameters such as alkali concentration, curing temperature, and activator type, thereby optimizing their performance for various construction applications [22, 23].However, challenges arise when using copper tailings for alkali activation, including variability in tailing composition and concerns about long-term environmental safety, particularly the potential leaching of heavy metals [24].

Building on existing research, this study aimed to develop novel alkali-activated artificial aggregates incorporating copper tailings. To address challenges such as compositional variability and strength reduction, a granulation process was proposed to produce consistent, high-quality aggregates. By combining granulation with alkali activation, this study seeks to advance sustainable solutions for waste utilization in construction and promote the industrial application of copper tailing-based artificial aggregates.

II. MATERIALS AND METHODS

2.1. Raw Materials

In this study, artificial aggregates were developed using alkali-activated CT with or without GGBS. Solid sodium silicate was used as the alkali activator. The copper tailings were sourced from Zhongtiaoshan Non-ferrous Metals Group, Shanxi, China. The as-received copper tailings were washed three times with tap water to avoid the possible influence of admixtures used during their production. After washing, the copper tailings were oven-dried for future use. GGBS was collected from Henan Guyou Engineering Testing Co.,Ltd. Fig.1 shows the scanning electron microscopy (SEM) images of CT and GGBS. Both GGBS and CT particles exhibited angular and irregular shapes.

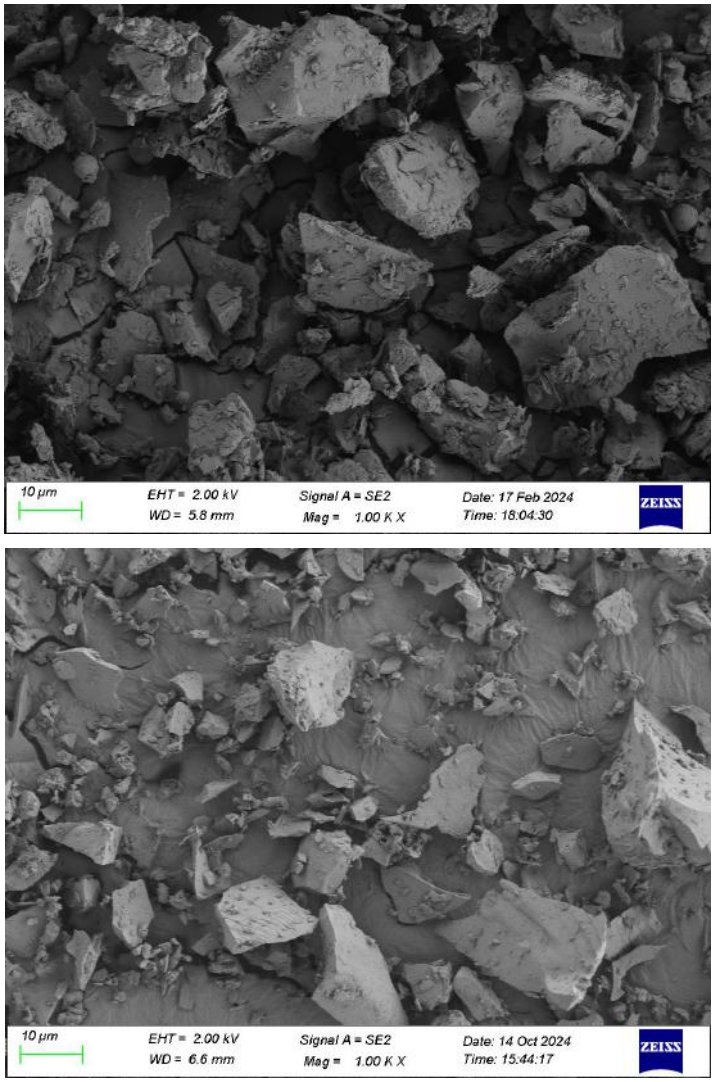

Fig.1: Morphology of CT and GGBS

Fig. 2 shows both the differential and cumulative particle size distributions of the copper tailings, measured using a laser particle size analyser (LS-POP(9), OMEC). According to Fig. 2a, nearly all CT particles are smaller than 300 µm. The differential particle size distribution shows a bimodal profile with two peaks at 18 µm and 125 µm. But the most frequent particle size of CT is 125 µm. Fig. 1b shows the particle size distribution of the GGBS. The most frequent particle size of GGBS is approximately 16 µm and nearly all particles are smaller than 50 µm. As shown in Fig. 2c, the particle size of the solid SS particles was comparable to that of CT. The most frequent particle size of SS is 260 µm and most of them are smaller than 600 µm.

Table. 1 shows the chemical compositions of the copper tailings and GGBS, as characterized by X-ray fluorescence (XRF). For CT, elements Si, Al, and Fe account for 81.0%. For GGBS, the major elements are Si, Ca, and Fe, which account for 85.8%. The alkali activator SS composed mainly of 50.23% sodium dioxide and 46.27% silicon dioxide in terms of chemical composition.

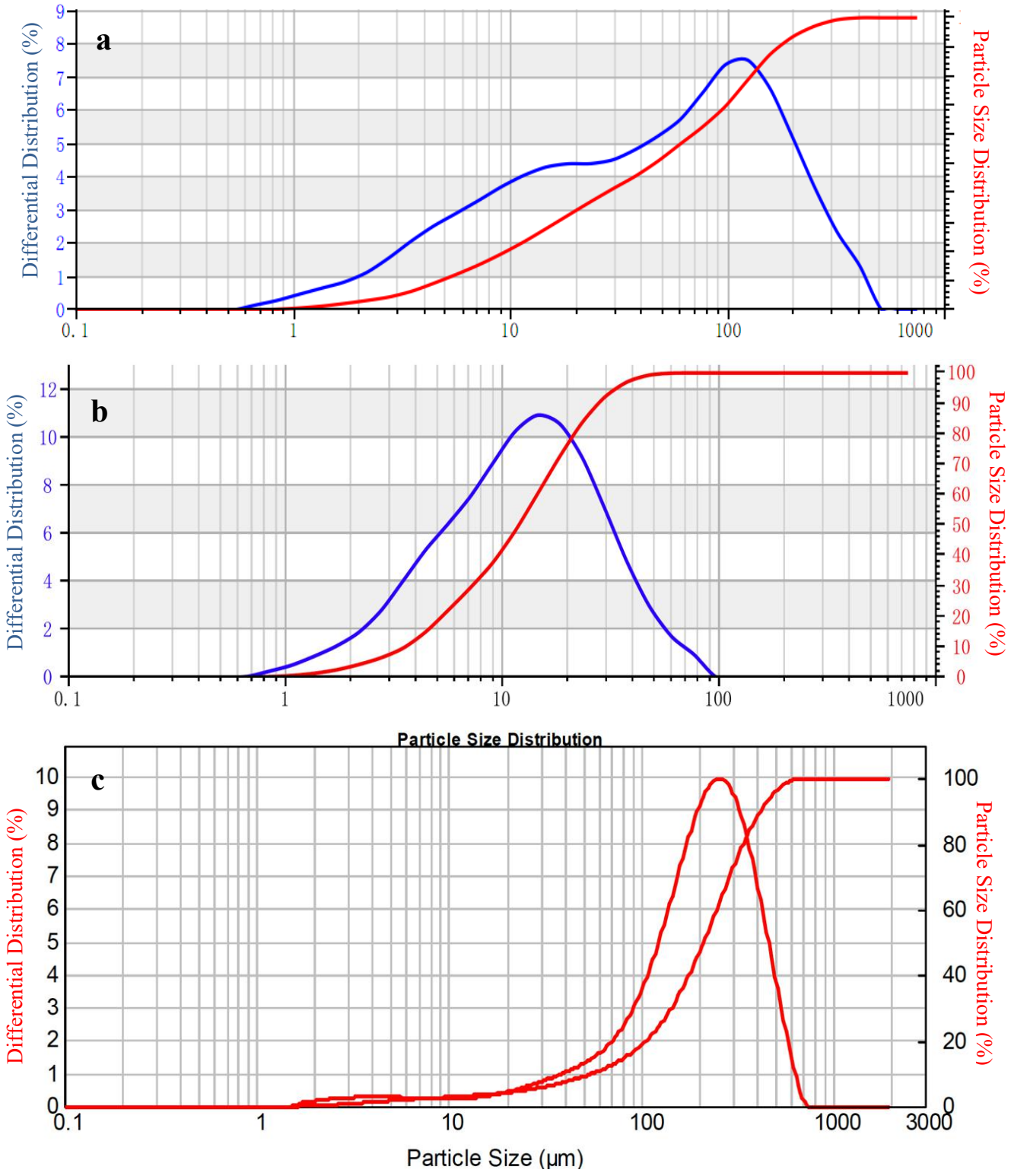

Fig. 2: Particle size distributions of CT, GGBS, and SS

Table.1: Chemical composition of copper tailing and GGBS

Oxides(%)	CT(%)	GGBS(%)
Si	58.301	34.20
Ca	4.575	34.00
Al	13.344	1.62
Fe	9.328	17.60
Mg	4.014	6.21
K	5.171	0.37
P	0.301	/
Cl	0.445	/
Ti	0.963	/
Mn	0.088	/
Cu	0.086	/
Rb	0.023	/
Sr	0.012	/
Zr	0.040	/

The X-ray diffraction (XRD) analysis was conducted by using a Empyrean (Malvern analytical)and phase identification was performed using the X'pertHighScore Plus software.Thediffraction patterns of CT and GGBS are presented in Fig. 3. According to the test results, the main crystalline phases in the CT were quartz (SiO_2), hedenbergite ($CaFeSi_2O_6$), calciumsulfate($CaSO_4$), calciumcarbonate($CaCO_3$), and anorthite ($CaAl_2Si_2O_8$). However, GGBS contains amorphous SiO_2 accordingtothe broad lump between 20°and35°shown in the spectrum.

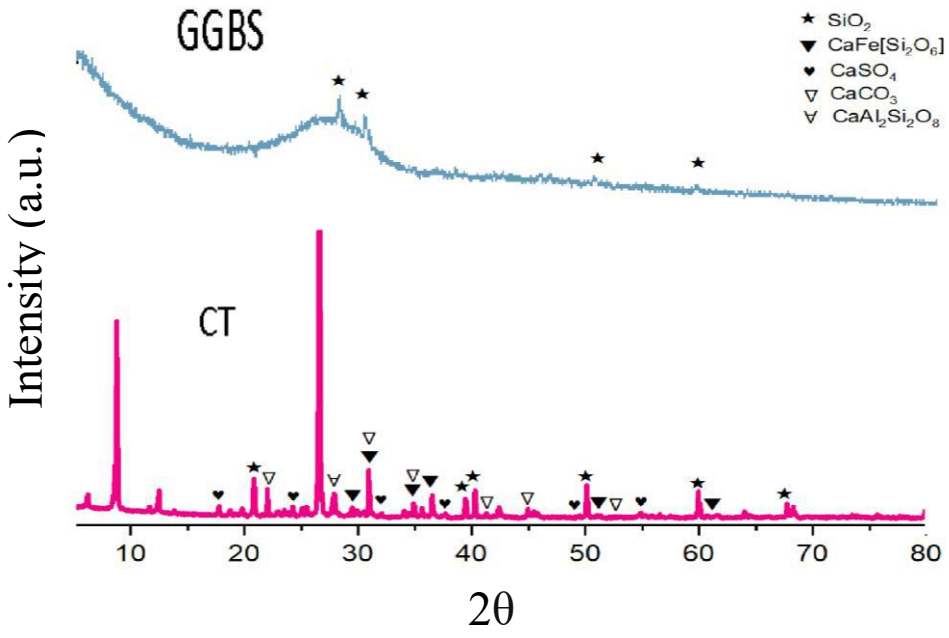

Fig. 3: XRD patterns of GGBS and CT

2.2. Sample preparations

The raw materials for preparing the artificial aggregates are copper tailings, GGBS, and solid sodium silicate. The copper tailings were first washed three times with tap water, oven-dried for 5h, and then mixed with GGBS and sodium silicate following the mixing proportions shown in Table 2. Five different mixes were prepared, as shown in the Table2, with various GGBS contents (10%, 20%, and 30%). The five mixes were denoted as CTS1, CTS2, CTBS10, CTBS20, and CTBS30. Previous research has shown that the incorporation of GGBS enhances the mechanical properties [25]. The dry materials were placed in a rotating disk granulator with speed of 20 rpm for 2 mins to ensure they can be mixed thoroughly. Then, the granulation process started as water was gradually and evenly sprayed onto the dry mixture using a watering bottle. Water addition, which is essential for proper moisture distribution, facilitates the binding process, aiding in the formation of granules [26]. Both the rotating speed and disk angle were adjusted to optimize granule formation according to established granulation principles [27]. As water was sprayed onto the mixture, the rotation speed was increased to 30 rpm. After 2 mins rotation, the speed was increased to 40 rpm and maintained for another 3 mins. The disk was inclined at a 45° angle, which was found to be optimal for granule production. The granulation process took approximately 7 min in current study. Fig. 4a shows the dry mixing of raw materials, while Fig. 4b and 4c show the granulation process with solid particles bound together to form fresh artificial aggregates.

Once granulation was completed, the aggregates were placed immediately in a sealed plastic container for curing. The curing process was conducted under temperature of 22 ± 1°C and relative humidity of 50 ± 5%. No thermal treatment was applied during the curing stage.

Fig. 4: Granulation process for artificial aggregates

Table 2: Mix proportions of artificial aggregate samples

Mixes	CT(g)	SS(g)	GGBS(g)	Water(g)	Water/binder	Water/SS
CTS1	1000	100	0	180	0.180	1.80
CTS2	1000	150	0	185	0.185	1.23
CTBS10	1000	100	100	195	0.177	1.95
CTBS20	1000	100	200	200	0.167	2.00
CTBS30	1000	100	300	210	0.162	2.10

2.3. Testing methods

2.3.1. Sieve analysis

The particle size distribution of the artificial aggregates was determined using a series of standard sieves with mesh openings of 5 mm, 10 mm, 14 mm, 20 mm, and 25 mm. This sieve analysis was conducted to quantify the range and proportion of aggregate sizes within each batch. The cumulative size distribution was calculated for each batch to provide a comprehensive profile of particle size variation. To ensure accurate and representative results, the size distribution tests were performed after the aggregates had undergone a 28-day curing period under controlled conditions, followed by 24 hours of air-drying to stabilize their moisture content [28]. This preparation minimized potential influences of residual moisture on the sieving process, enhancing the reliability of the measurements.

2.3.2. Oven dried density and water absorption measurement

Following a 28-day curing period under ambient conditions, the oven-dried density and water absorption properties of the synthetic aggregates were evaluated in accordance with established standards [29]. This assessment was conducted on approximately 500 g of aggregates with particle sizes ranging from 5 mm to 25 mm to ensure a representative sample.

The aggregates were submerged in water for 24 hours to achieve full saturation. After immersion, they were removed and dried to a saturated surface dry (SSD) condition using a dry cloth, and their mass was recorded as m1. The SSD aggregates were then placed in a 1 liter graduated cylinder, and water was incrementally added until the total volume reached 1 liter, following the procedure outlined in [30]. The combined mass of the aggregates, water, and cylinder was recorded as m2. Subsequently, the aggregates were transferred to an oven set at 105°C and dried until a constant mass was achieved, indicating complete moisture removal. This oven-dried mass was recorded as m3.

The oven-dried particle density, ρ (in kg/m³), was calculated using Equation 1:

$$\rho = \frac{m3}{m1-(m2-m4)} \times 1000 \quad (1)$$

Here, m4 represents the mass of the graduated cylinder filled with 1000 ml of water, serving as a reference for the volume displacement calculation.

Additionally, the water absorption capacity (Sw, expressed as a percentage) of the aggregates was determined using Equation 2, though the specific equation was not provided in the original text. For completeness, it is typically calculated as:

$$Sw = \frac{m1-m3}{m3} \times 100 \quad (2)$$

2.3.3. Crushing strength of individual artificial aggregate

The compressive strength of the artificial aggregates was assessed following the methodology outlined in prior research [32]. Testing was conducted after curing periods of 3, 7, and 28 days to evaluate strength development over time. A 600 kN universal testing machine (SHT4605, MTS) was employed, and a minimum of 20 aggregates from each sample type were tested to ensure statistical reliability.

The aggregates were subjected to a controlled loading rate of 0.6 mm/min to achieve consistent and reproducible results. The compressive strength of individual aggregates, denoted as σ(in MPa), was calculated using the equation 3 provided in [33]:

$$\sigma = \frac{2.8 \times F}{\pi \times d^2} \quad (3)$$

where the individual strength (σ) is defined as the ratio of the peak load (F) recorded at the crushing failure of the aggregate to the distance (d) between the two connection points of the aggregates with the load cell and the supporting base (where the aggregate rests on the supporting base).

2.3.4. SEM observations

A ZEISS Gemini 300 scanning electron microscope (SEM) was used for microstructure observations in the present work. The samples for SEM were collected from crushed artificial aggregates after mechanical tests. Before SEM observation, the SEM samples were dried in a vacuum oven for 8h.

2.3.5. XCT observations

A dual-tube micro-focus X-ray computed tomography (XCT) system (Phoenix V|tome|x S 240) was employed to analyze the pore distribution within the aggregates after 28 d curing. The XCT testing parameters were set to an X-ray tube voltage of 140 kV, current of 45 μA, and spatial resolution of 10 μm. Further details on the system and methodology are provided in the following sections.

III. RESULTS AND DISCUSSION

3.1. Size distribution of artificial aggregates

The typical size distribution of artificial aggregates can vary depending on the production method and material type, and particle sizes have ranged from as small as 4 mm to as large as 20 mm [17]. From previous research studies, artificial aggregates produced through different methods using waste materials typically range from 4 mm to 20 mm in size [21, 34, 35]. The most commonly reported size range is 5–16 mm. Some studies have successfully produced smaller aggregates of approximately 2.36–4.75 mm [35], whereas others have achieved larger sizes of up to 25 mm. Based on the sieve analysis, the artificial aggregates produced in current study showed varying size distributions across different samples. The most dominant size was 10.0 mm, comprising 51.17%–59.37% of the total distribution. The samples also contained 5.0 mm aggregates, particularly notable in CTBS1 and CTBS30 with proportions of 30.88% and 36.09%, respectively. A distinct characteristic was observed in CTS2, which contained 14.0 mm aggregates, accounting for 22.34% of its composition.TheCTBS10 sample demonstrated a more uniform distribution between 5.0 mm and 10.0 mm sizes (42.13% and 51.17%), while CTBS20 showed a broader range, including some 20.0 mm aggregates at 3.6%.Small amounts of 2.5 mm aggregates were also present,

indicating some variation in the process. These findings align with previous research on artificial aggregates from waste materials such as fly ash and slag, which typically show size distributions ranging from 4.75 to 20 mm [36], with a preference for sizes of approximately 10 mm for construction applications. The presence of both very fine (2.5 mm) and larger (20 mm) particles suggests some variability in the granulation process control, similar to the observations in previous studies using materials such as steel slag and recycled concrete aggregates.

Table.3: Size distribution of artificial aggregate samples.

Mix ID	2.5mm	5.0mm	10.0mm	14.0mm	20.0mm	25.0mm
CTS1	4.41%	30.88%	59.37%	5.32%	0%	0%
CTS2	0.55%	20.61%	56.53%	22.34%	0%	0%
CTBS10	1.82%	42.13%	51.17%	4.87%	0%	0%
CTBS20	3.01%	33.93%	51.24%	8.2%	3.6%	0%
CTBS30	2.77%	36.09%	57.4%	3.73%	0%	0%

3.2. Oven-dried density of artificial aggregates

The oven-dried density of the different artificial aggregates, as shown in Fig. 5, reveals variations in density resulting from different mix proportions.BothCTS1 and CTS2 showed lower oven-dried densities than CTBS10, CTBS20, and CTBS30. The oven-dried particle density of CTS1 was 750 kg/m³, while CTS2 showed a slightly lower density of683 kg/m³. For the samples with GGBS, the densities of CTBS10 and CTBS20 were 1287.07 and 1295 kg/m^3, respectively. The sample CTBS30 had the highest oven-dried density of 1328.65 kg/m^3.Therefore, according to the results, the addition of GGBS can increase the density of artificial aggregates developed using the granulation process. This can be attributed to the finer particle size of GGBS, which improved the compactness of the artificial aggregate during granulation. Based on previous research, artificial aggregates produced from various waste materials have shown diverse density values depending on the production method and raw materials used. Cold-bonded artificial aggregates typically exhibit densities ranging from 1600 to 2200 kg/m³[37, 38], particularly when produced from materials such as fly ash and slag [39]. Aggregates produced using the pelletization method commonly show densities ranging from 1800 to 2400 kg/m³[40, 41].It was found that the density of artificial aggregates prepared by using granulation are lower compared to other methods.

The theoretical density of an artificial aggregate can be calculated using the real density of each constituent. The densities of CT, GGBS, SS, and water were assumed to be 2500 kg/m³, 2900 kg/m^3, 1440 kg/m³, 1.0 kg/m³, respectively. Following the principle of additive volumes, if perfect packing is assumed, the estimated theoretical density for each sample can be calculated. The theoretical densities of CTS1 and CTS2 were 1970 kg/m^3 and 1940 kg/m^3, respectively. The theoretical densities of CTBS10, CTBS20, and CTBS30 were 1995 kg/m^3, 2030 kg/m^3, and 2060 kg/m^3, respectively. Theoretically, there is no significant difference in density between the two types of samples. However, the experimentally measured oven-dried densities for the samples were significantly lower than the theoretical values, and the changing trend for the samples was consistent with the theoretical calculations. This discrepancy arises primarily due to the presence of porosity and void spaces within the granulated artificial aggregates, with estimated porosities of approximately 62% and 64.7% for CTS1 and CTS2, respectively, and approximately 35-36% for CTBS10, CTBS20, and CTBS30.Additional factors contributing to the lower measured densities include incomplete granulation, lower packing efficiency, uneven binder distribution, and potential hydration reactions during granulation, which introduce extra voids. These differences highlight the need to optimize the granulation process to minimize porosity and enhance packing density, thereby improving the alignment between theoretical predictions and experimental measurements.

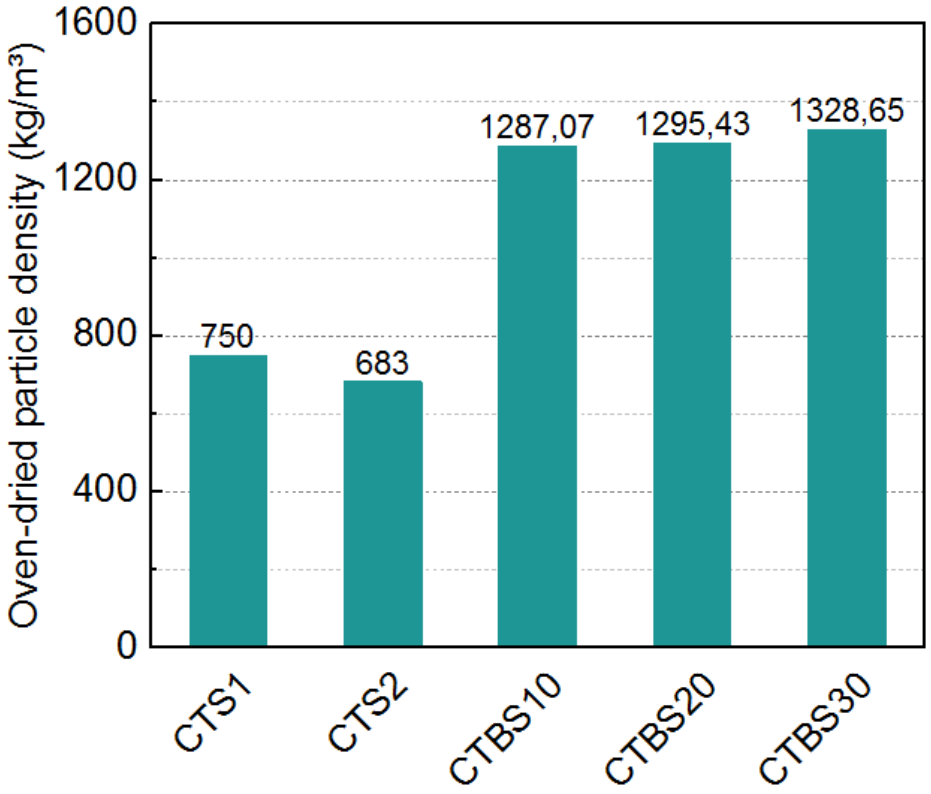

Fig. 5: Oven-dried density of the artificial aggregates

3.3. Water absorption

The water absorption of aggregates is a key indicator of their internal pore structure, with higher absorption typically reflecting greater porosity, which can compromise aggregate performance [42]. Fig. 6 presents the water absorption results for the CTS and CTBS aggregate samples, ranging from 10.22% to 12.61%. These values compare favorably to those reported in previous studies using similar methods (10–30% for sintered and cold-bonded artificial aggregates [43,44] and 8–25% for pelletized artificial aggregates [45,46], indicating relatively lower porosity in the tested samples [37,46].Among the samples, CTS1 and CTS2 exhibited the highest water absorption at 12.30% and 12.61%, respectively. In contrast, the CTBS series showed a progressive decrease in water absorption with increasing ground granulated blast-furnace slag (GGBS) content: CTBS10 at 10.65%, CTBS20 at 10.44%, and CTBS30 at 10.22%. This trend suggests that GGBS enhances hydration and pozzolanic reactions, promoting a denser microstructure with reduced porosity [18].

Water absorption in aggregates is primarily governed by the presence of mesopores (2–50 nm) and macropores (>50 nm), which facilitate capillary action and bulk water uptake, respectively. Mesopores contribute to water retention due to their high surface area, while macropores enable greater water infiltration through larger void spaces. The elevated water absorption in CTS1 and CTS2 corresponds to their lower oven-dried densities (750 kg/m³ and 683 kg/m³, respectively), indicating a higher volume of connected meso and macropores. Conversely, the CTBS series, with higher oven-dried densities (1287–1328 kg/m³) and lower water absorption, reflects reduced porosity, likely due to improved particle packing and pore-filling effects from GGBS incorporation.

The observed inverse relationship between water absorption and oven-dried density in the CTBS series aligns with established literature, which indicates that denser aggregates exhibit lower porosity and, consequently, reduced water absorption [18,47,48]. This correlation underscores the influence of mixture composition and granulation processes on pore structure. Specifically, the incremental addition of GGBS in the CTBS series appears to minimize capillary pore volume, enhancing structural integrity and reducing water uptake.

These findings highlight the potential to tailor aggregate properties by optimizing GGBS and binder proportions, enabling the design of artificial aggregates with controlled porosity for specific applications. Further investigation into the interplay between pore size distribution, density, and mechanical performance could enhance the understanding of these relationships.

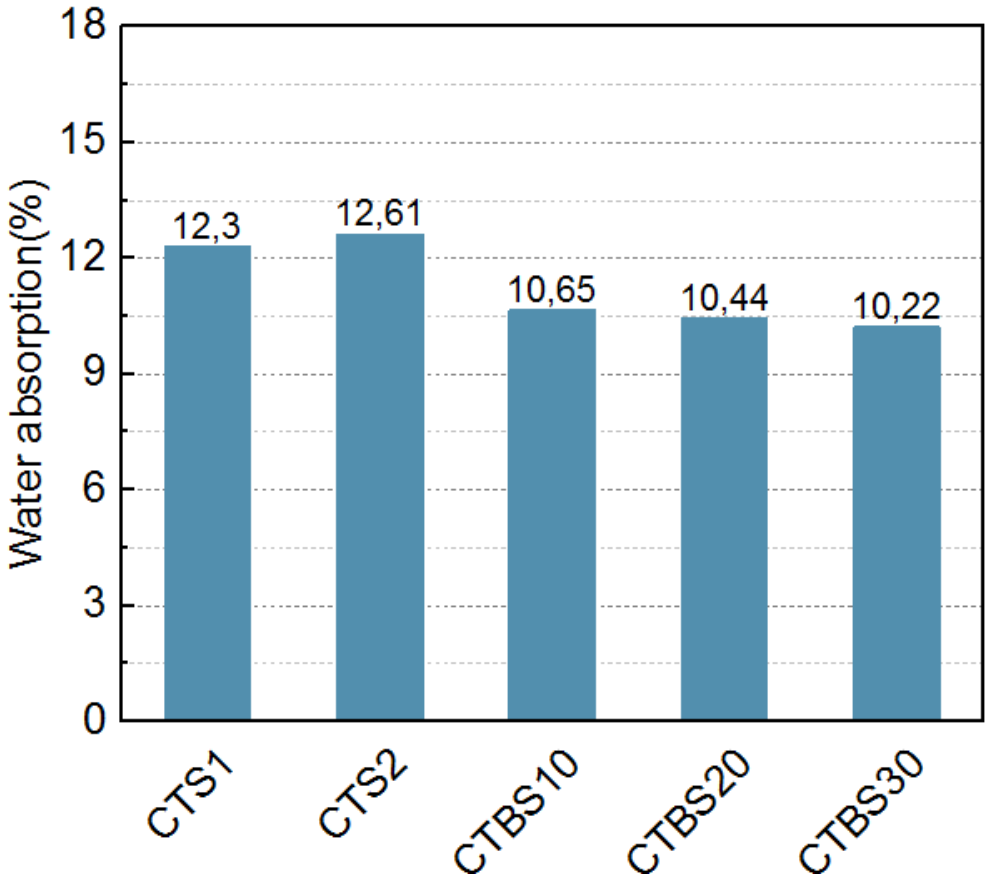

Fig. 6: Water absorption of the artificial aggregate samples

3.4. Crushing strength

Previous studies indicate that the crushing strength of artificial aggregates (AAs) typically falls below 10 MPa [48], with sintered AAs ranging from 3 to 25 MPa and cold-bonded or pelletized AAs from 0.4 to 22.7 MPa [36,43,49,50]. Fig. 7 illustrates the strength development of the tested AA samples over curing periods of 3, 7, and 28 days. At 3 days, the average crushing strength ranged from 1.2 to 3.0 MPa; at 7 days, from 2.5 to 4.7 MPa; and at 28 days, from 3.7 to 5.8 MPa. These results compare favorably to prior studies using similar methods [34,46].

All samples exhibited progressive strength gains with curing time, with distinct differences between the CTS and CTBS series. The CTS samples (CTS1 and CTS2) showed moderate strength increases, reaching 3.5 MPa and 1.7 MPa at 28 days, respectively. Notably, CTS2 exhibited lower strength than CTS1 despite higher sodium silicate (SS) content, suggesting that increased SS does not consistently enhance strength. In contrast, the CTBS samples demonstrated superior strength at both early and later curing stages. The incorporation of ground granulated blast-furnace slag (GGBS) markedly improved performance, with CTBS10, CTBS20, and CTBS30 achieving 28-day strengths of 4.0 MPa, 5.0 MPa, and 5.8 MPa, respectively. This trend indicates that higher GGBS content enhances strength development, likely due to reduced porosity, as observed in prior analyses. The lower porosity of the CTBS series, compared to the CTS series, correlates strongly with their enhanced mechanical properties. Thus, the combination of GGBS with copper tailings and sodium silicate significantly improves the crushing strength and structural integrity of these artificial aggregates.

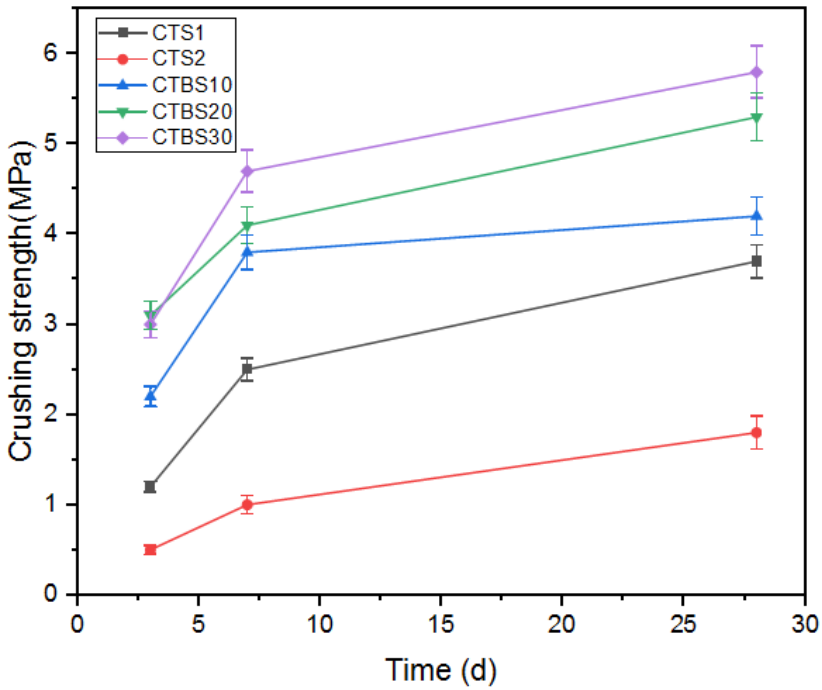

Fig. 7: The crushing strength of the artificial aggregate samples

3.5. Individual artificial aggregate strength

To assess the variability in individual granule strength of artificial aggregates after 28 days, which exhibited significant scattering, the Weibull distribution was applied using Equation 4 [27]:

$$F(\sigma) = 1 - [-\left(\frac{\sigma}{\lambda}\right)^{k}] \quad (4)$$

where $F(\sigma)$ is the cumulative distribution function of individual granule strength, σ is the granule strength, λ is the Weibull scale parameter (characteristic strength), and k is the Weibull shape parameter (indicating strength uniformity). The fitting results are presented in Table 4, with the corresponding Weibull cumulative distribution curves for the five mixes (CTS1, CTS2, CTBS10, CTBS20, CTBS30) shown in Fig 8.

Table 4 indicates coefficients of determination exceeding 0.95 for all mixes, confirming excellent fits of the Weibull model to the granule strength data. The distribution curves (Fig. 8) reveal distinct patterns among the mixes. CTS2, with 150 g sodium silicate, exhibited the lowest strength, with most granules failing below 2 MPa. In contrast, CTS1 (100 g sodium silicate) showed improved performance, with failures concentrated around 4 MPa. The incorporation of ground granulated blast-furnace slag (GGBS) in the CTBS series significantly enhanced granule strength, as evidenced by a rightward shift in the distribution curves. CTBS10 displayed strengths primarily between 4 and 5 MPa, while CTBS20 and CTBS30, with higher GGBS contents, achieved strengths of 6–8 MPa.

The curve shapes provide further insight into strength uniformity. CTS2's steep curve reflects consistent but low strength, indicating uniform but weak granules. The CTBS series exhibited more gradual curves, suggesting greater strength variability, particularly for CTBS10. However, CTBS20 and CTBS30 maintained similar distribution shapes with progressively higher strengths, indicating that increased GGBS content enhances strength without sacrificing uniformity. Notably, CTBS10, CTBS20, and CTBS30 showed larger scattering in strength values compared to CTS1 and CTS2, potentially due to GGBS incorporation, though this hypothesis requires further investigation.

These findings demonstrate that excessive sodium silicate (CTS2) compromises granule strength, whereas increasing GGBS content systematically improves strength, with CTBS30 achieving the highest values. The Weibull analysis underscores the role of mix composition in controlling both strength and its variability, offering valuable insights for optimizing artificial aggregate design.

Table.4: Size distribution of the artificial aggregates

Sample	K	Λ (MPa)	R2
CTS1	7.42	4.06	0.962
CTS2	3.86	1.99	0.983
CTBS10	4.64	4.49	0.998
CTBS20	4.88	5.77	0.991
CTBS30	4.71	6.1	0.995

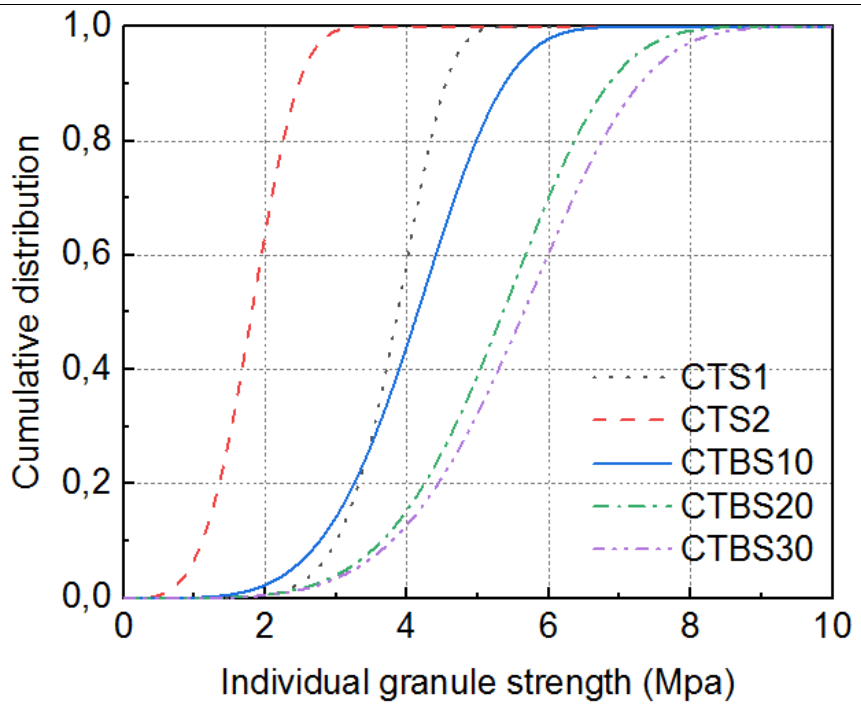

Fig. 8: The Weibull cumulative distribution curves of the individual granule strength of the aggregates

3.6. SEM

Figure 9 presents scanning electron microscopy (SEM) images of the artificial aggregate samples. The CTBS samples exhibited a denser and more compact microstructure compared to the CTS samples at both low and high magnifications. Cracks were more prevalent in the CTS samples, suggesting poor bonding between phases. In contrast, the CTBS samples displayed a cohesive microstructure with well-integrated phases, consistent with their lower water absorption and reduced porosity relative to the CTS samples, as reported earlier.

Figure 10 shows energy-dispersive X-ray (EDX) mapping of Si, Al, Na, and Ca in CTS10 and CTBS30 samples. In CTS10 (Fig. 10a), an unreacted copper tailing (CT) particle is evident, characterized by a high Si concentration with minimal Al, Na, or Ca, indicating low reactivity of the CT material. In the CTS samples, CT primarily served as a filler rather than anreactive component. In CTBS30 (Fig. 10b), regions rich in Na, Si, and Al, but lacking Ca, suggest the formation of sodium alumino silicate hydrate (N-A-S-H) gel, driven by alkali activation of GGBS with sodium silicate. Notably, calcium silicate hydrate (C-S-H) gel was not prominently observed in the CTBS samples. These findings indicate that the alkali-activated GGBS products acted as a binding phase, enhancing the microstructural integrity of the CTBS samples, which aligns with their improved mechanical properties and reduced porosity.

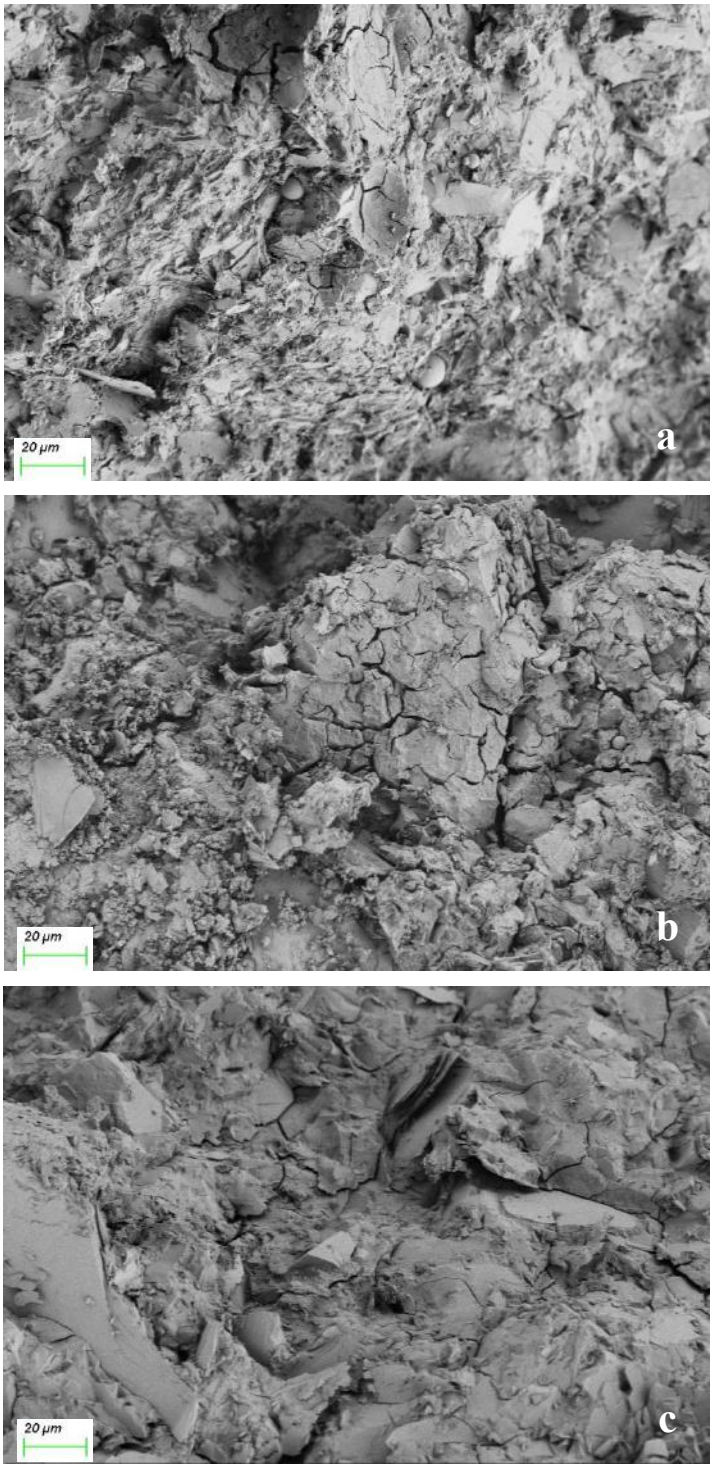
20 µm
a
20 µm
b
20 µm
c

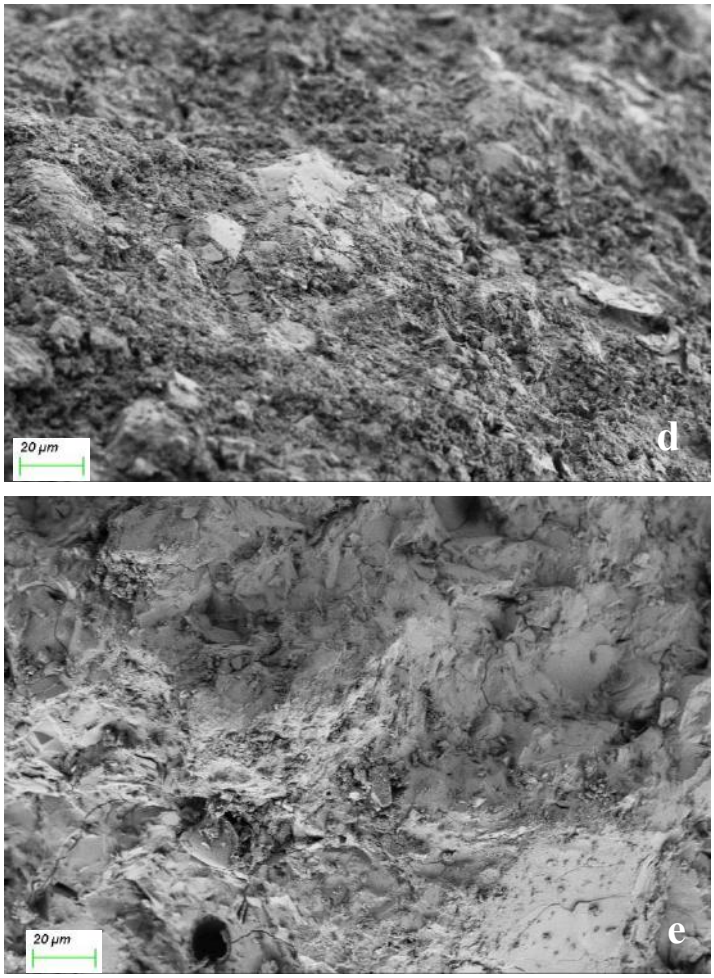

Fig. 9: SEM images of CTS1(a), CTS2 (b), CTBS10 (c), CTBS20 (d), and CTBS30 (e).

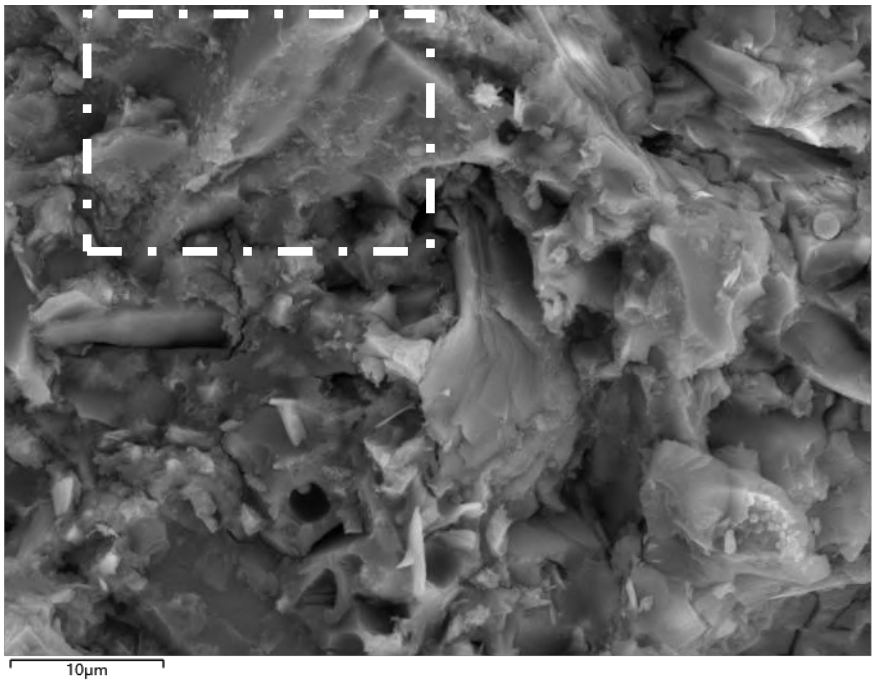

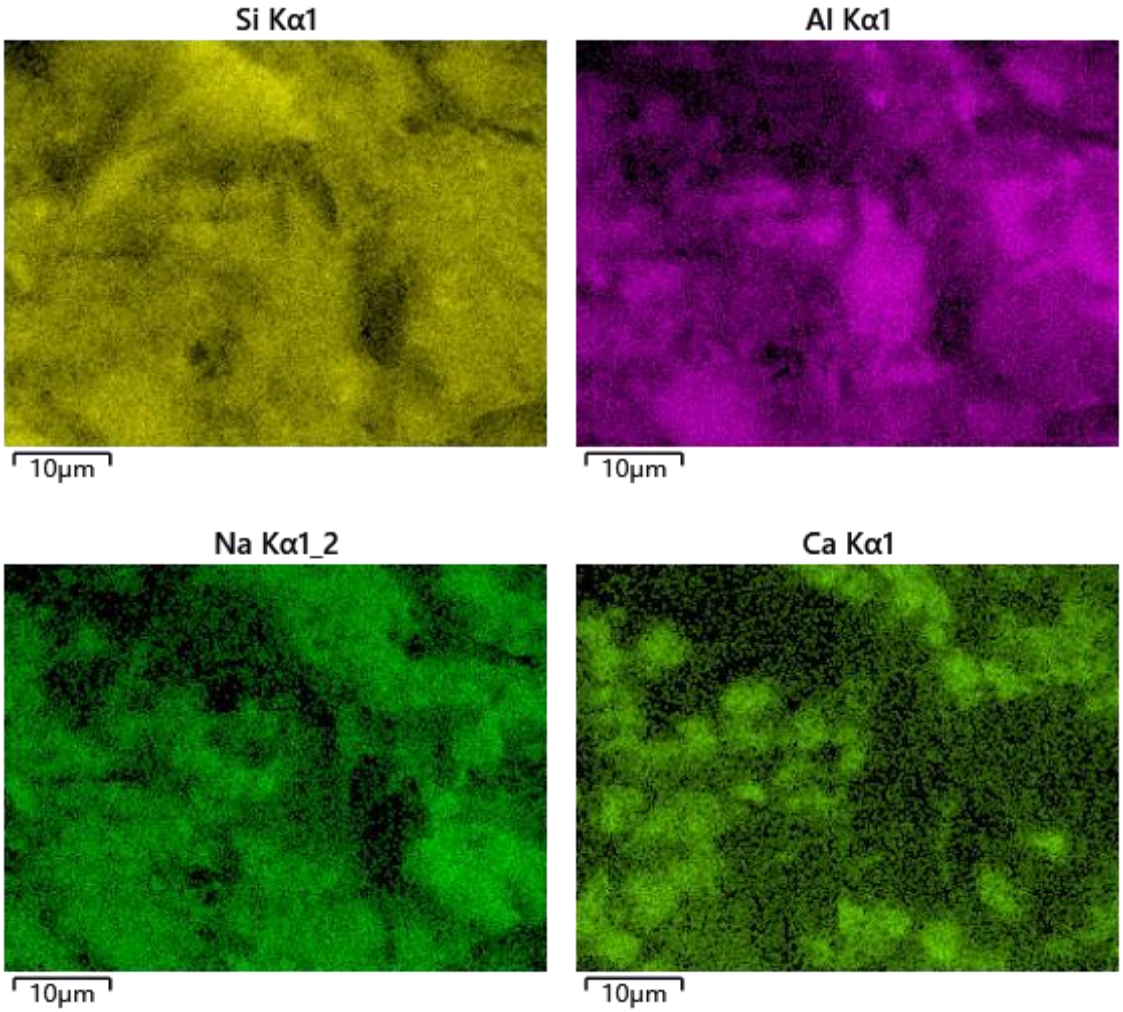
Si Kα1
10µm
Al Kα1
10µm
Na Kα1_2
10µm
Ca Kα1
10µm

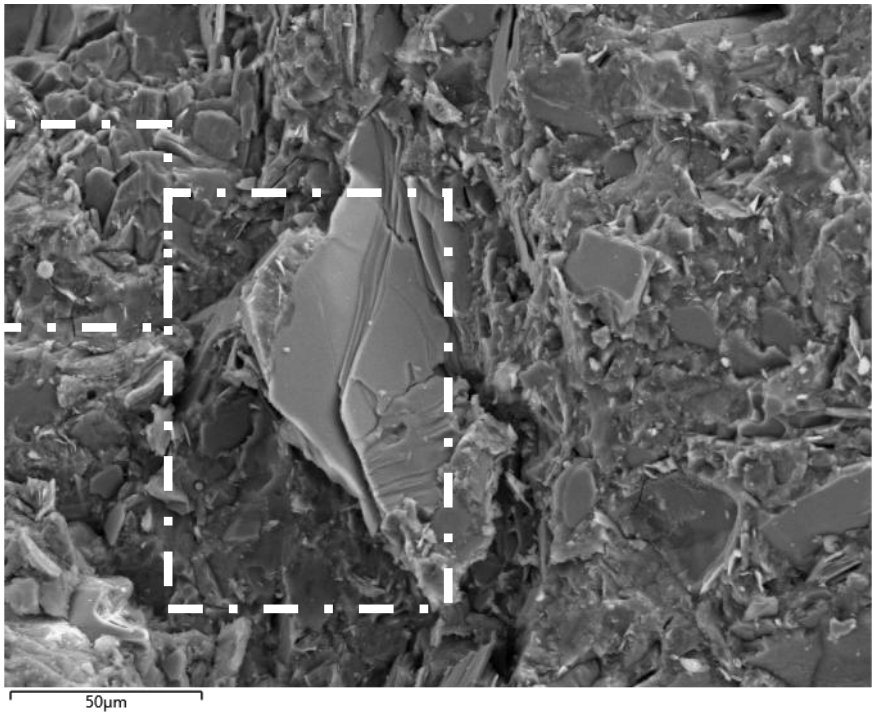
50µm

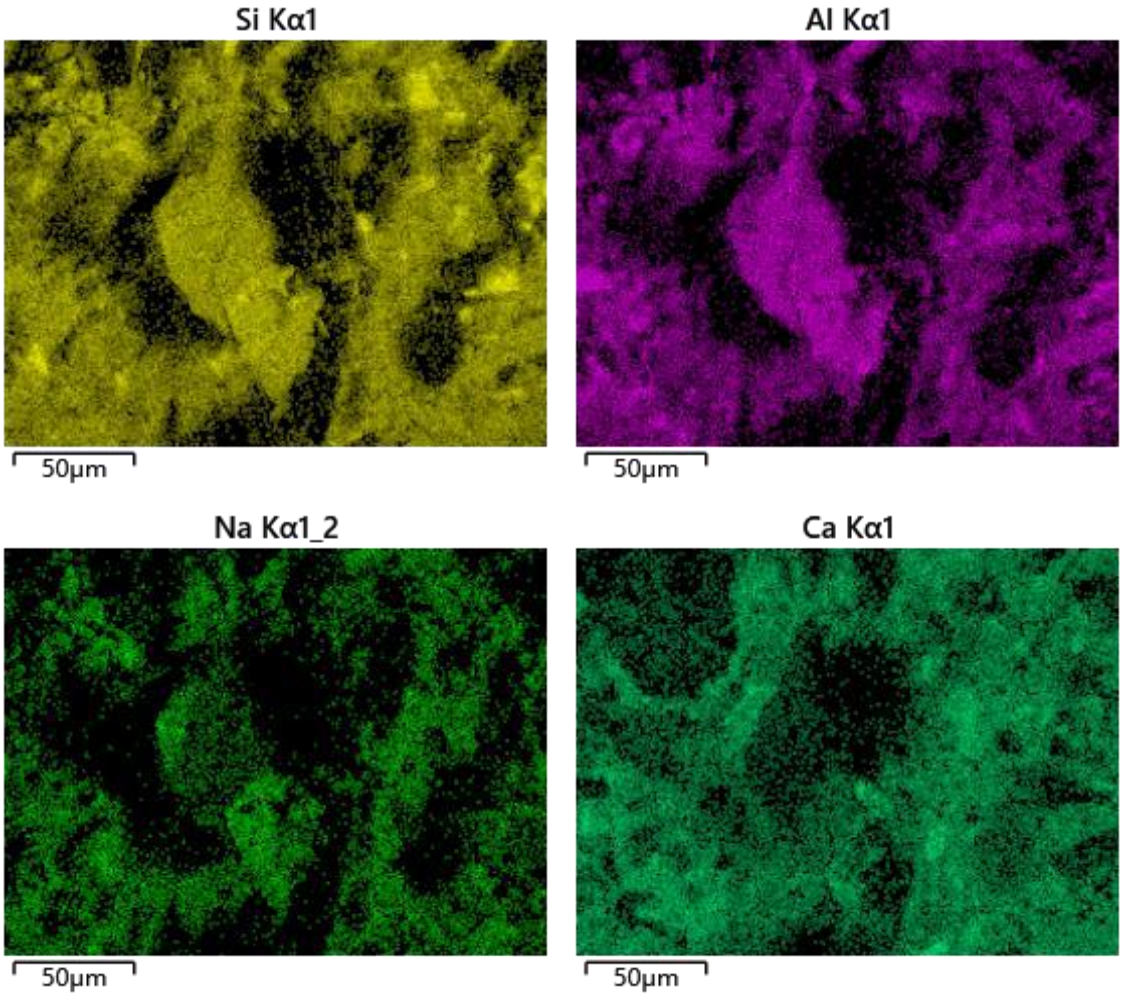

Fig. 10: EDX images of CTS and CTBS sample

3.7. XCT analysis

The internal pore structure of the artificial aggregates was studied using XCT. Fig. 11 shows the CT images of the CTS and CTBS samples. The XCT scans can only reveal pores larger than 1µm due to equipment resolution constraints. The visible pores in the images represent either air voids created during granulation or cavities formed by the dissolution of sodium silicate.TheCTS1 and CTS2 samples, which do not contain GGBS, exhibit a higher number of larger pores when observed visually. The big pores with irregular shape are voids formed by dissolution of SS. In contrast, the CTBS samples with the addition of GGBS showed a more refined pore structure with smaller and more evenly distributed pores. There are fewer pores with irregular shapes and more spherical pores, indicating a high degree of reaction of SS. In addition, as the GGBS content increased from CTBS10 to CTBS30, the pore structure became more uniform, and the size and frequency of large pores decreased. Especially the CTBS30, it exhibited the smallest and most uniformly distributed pores, which is consistent with the crushing strength test results. The increased crushing strength of the CTBS samples with higher GGBS content can be attributed to this refined pore structure, as observed in the XCT images.

However, the granulation process can be further improved to produce more compact artificial aggregates by adjusting the particle size distribution of the raw materials and improving the reactions between them.

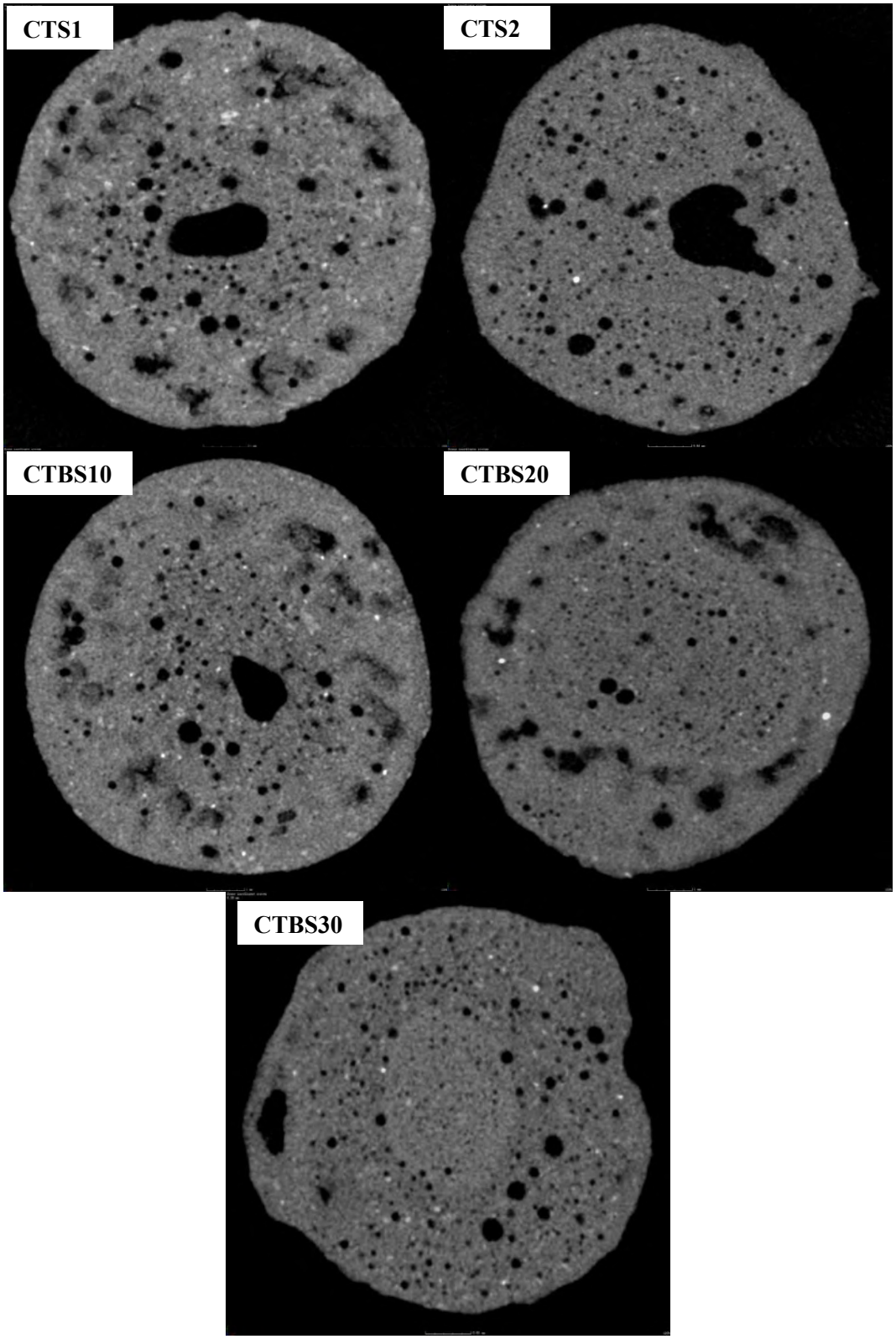

Fig. 11: XCT images of the aggregate samples

IV. CONCLUSION

The study demonstrates that copper tailings can be recycled into sustainable artificial aggregates using a granulation process activated by sodium silicate. Incorporating GGBS significantly enhances the aggregates' properties by increasing density, reducing water absorption, and improving crushing strength. The microstructural analyses, including SEM and XCT, revealed that GGBS

facilitates the formation of a denser and more uniformly bonded matrix through N-A-S-H gel formation and pore refinement, thereby substantiating the potential of this method for developing eco-friendly construction materials while optimizing mechanical performance.

Granulation excels among artificial aggregate preparation methods through its efficiency and cost-effectiveness. Unlike sintering or cold bonding, it forms aggregates via mechanical rolling with minimal energy. The process produces quasi-spherical granules with good properties while controlling size and shape, making it ideal for fine materials like copper tailings. Compared to energy-intensive sintering and shape-limited extrusion, granulation provides an optimal balance of simplicity and quality output.

Current approach not only addresses the environmental concerns associated with copper tailings disposal but also offers a viable solution for the construction industry's growing demand for sustainable materials. Future studies could explore the long-term durability of these aggregates in various construction applications, as well as investigate the potential for scaling up this process for industrial-scale production.

ACKNOWLEDGEMENT

The authors are grateful for the financial support from the National Natural Science Foundation of China (Grant No. 52178238).

REFERENCES

[1] Shengo, L. M. (2021). Review of practices in the managements of mineral wastes: The case of waste rocks and mine tailings. *Water Air Soil Pollution, 232(8), 273.* https://doi.org/10.1007/s11270-021-05198-w

[2] Chen, S.-C., Gao, M.-Y., Lin, W.-T., Liang, J.-F., & Li, D.-W. (2022).Effects of incorporating large quantities of copper tailings with various particle sizes on the strength and pore structure of cement-based materials. *Construction and Building Materials, 329, 127150.* https://doi.org/10.1016/j.conbuildmat.2022.127150

[3] Pilegis, M., Gardner, D., & Lark, R. (2016). An investigation into the use of manufactured sand as a 100% replacement for fine aggregate in concrete. *Materials, 9(6), 440.* https://doi.org/10.3390/ma9060440

[4] Mary, J. A. (2016). An experimental investigation on copper slag as replacement of fine aggregate in concrete. *International Journal of Civil Engineering and Technology, 7(6), 282-289.* http://iaeme.com/Home/issue/IJCIET?Volume=7&Issue=6

[5] Bekkeri, G. B., Shetty, K. K., & Nayak, G. (2023). Producing of alkali-activated artificial aggregates by pelletization of fly ash, slag, and seashell powder. *Innovative Infrastructure Solutions, 8, 258.* https://doi.org/10.1007/s41062-023-01227-1

[6] Stempkowska, A., & Gawenda, T. (2024). Artificial lightweight aggregate made from alternative and waste raw materials, hardened using the hybrid method. *Scientific Reports, 14, 16880.* https://doi.org/10.1038/s41598-024-67454-3

[7] Wibowo, A. P., Saidani, M., & Khorami, M. (2024). Enhancing sustainability in construction: Investigating the thermal advantages of fly ash-coated expanded polystyrene lightweight concrete. *Journal of Composites Science, 8(4), 157. https://doi.org/10.3390/jcs8040157*

[8] Basa, B., Pradhan, N., & Parhi, L. P. (2020). Mechanical properties of concrete with sintered fly ash aggregate as substitute of natural fine aggregate. *IOP Conference Series: Materials Science and Engineering, 970(1), 012013. https://doi.org/10.1088/1757-899X/970/1/012013*

[9] Ren, Z., & Li, D. (2023). Application of steel slag as an aggregate in concrete production: A review. *Materials, 16(17), 5841. https://doi.org/10.3390/ma16175841*

[10] Gebremariam, H. G., Taye, S., & Tarekegn, A. G. (2024). Parent concrete strength effects on the quality of recycled aggregate concrete: A review. *Heliyon, 10(4), e26212. https://doi.org/10.1016/j.heliyon.2024.e26212*

[11] Whwah, M. S., Mahmmod, L. M. R., Abdoulhaleem, H. H., et al (2024). Internal curing utilising recycled concrete aggregate: A sustainable approach for improving high-strength concrete's performance. *Arabian Journal for Science and Engineering. Advance online publication. https://doi.org/10.1007/s13369-024-09187-z*

[12] Ismail, L., Abdel Razik, M., Ateya, E., [list all authors if et al (2024). Optimizing sustainable concrete mixes with recycled aggregate and Portland slag cement for reducing environmental impact. *Discover Materials, 4, 68. https://doi.org/10.1007/s43939-024-00136-z*

[13] Collivignarelli, M. C., Cillari, G., Ricciardi, P., Miino, M. C., Torretta, V., Rada, E. C., & Abbà, A. (2020). The production of sustainable concrete with the use of alternative aggregates: A review. *Sustainability, 12(19), 7903. https://doi.org/10.3390/su12197903*

[14] Singh, N., & Raza, J. (2024). Life cycle analysis of light weight artificial aggregates for sustainable construction. *Proceedings of the International Conference on Civil, Structural and Transportation Engineering. https://doi.org/10.11159/iccste24.171*

[15] Bamigboye, G. O., Ademola, D., Kareem, M., Orogbade, B., Odetoyan, A., & Adeniyi, A. (2022). Durability assessment of recycled aggregate in concrete production. In P. O. Awoyera, C. Thomas, & M. S. Kirgiz (Eds.), *The structural integrity of recycled aggregate concrete produced with fillers and pozzolans (pp. 445–467). Woodhead Publishing. https://doi.org/10.1016/B978-0-12-824105-9.00010-X*

[16] Hongling, Q., Suimin, M., & Xincong, Z. (2010). Environmental impact assessment of artificial aggregate systems based on fuzzy comprehensive evaluation. *2010 International Conference on Challenges in Environmental Science and Computer Engineering (pp. 420–423). IEEE. https://doi.org/10.1109/CESCE.2010.35*

[17] Bekkeri, G. B., Shetty, K. K., & Nayak, G. (2024). Production of artificial aggregates and their impact on properties of concrete. In R. K. Pancharathi, C. K. Y. Leung, & J. M. Chandra Kishen (Eds.), *Low carbon materials and technologies for a sustainable and resilient infrastructure (pp. 359–370). Springer. https://doi.org/10.1007/978-981-99-7464-1_26*

[18] Gesoğlu, M., Güneyisi, E., & Öz, H. Ö. (2012). Properties of lightweight aggregates produced with cold-bonding pelletization of fly ash and ground granulated blast furnace slag. *Materials and Structures, 45, 1535–1546. https://doi.org/10.1617/s11527-012-9855-9*

[19] Sharath, B. P., & Das, B. B. (2021). Production of artificial aggregates using industrial by products admixed with mine tailings A sustainable solution. In B. B. Das, S. V. Nanukuttan, A. K. Patnaik, & N. S. Panandikar (Eds.), *Recent trends in civil engineering (Vol. 105, pp. 433–443). Springer. https://doi.org/10.1007/978-981-15-8293-6_33*

[20] Araujo, F. S. M., Taborda-Llano, I., Nunes, E. B., & Santos, R. M. (2022). Recycling and Reuse of Mine Tailings: A Review of Advancements and Their Implications. *Geosciences, 12(9), 319. https://doi.org/10.3390/geosciences12090319*

[21] Bekkeri, G. B., Shetty, K. K., & Nayak, G. (2024). Performance of concrete produced with alkali-activated artificial aggregates. *Journal of Materials Cycles and Waste Management, 26, 2024–2042. https://doi.org/10.1007/s10163-024-01938-2*

[22] Falah, M., Obenaus-Emler, R., Kinnunen, P., & Illikainen, M. (2020). Effects of activator properties and curing conditions on alkali-activation of low-alumina mine tailings. *Waste and Biomass Valorization, 11, 5027–5039. https://doi.org/10.1007/s12649-019-00781-z*

[23] Pradhan, S. S., Mishra, U., Biswal, S. K., & Sahoo, T. (2024). Development of sustainable slag-based alkali-activated concrete incorporating fly ash at ambient curing conditions. *Energy, Ecology and Environment, 9, 563–577. https://doi.org/10.1007/s40974-024-00319-7*

[24] Esmaeili, J., & Aslani, H. (2019). Use of copper mine tailing in concrete: Strength characteristics and durability performance. *Journal of Materials Cycles and Waste Management, 21, 729–741. https://doi.org/10.1007/s10163-019-00831-7*

[25] Noufal, E., Kasthurba, A., & Sudhakumar, J. (2021). Influence of copper slag and GGBS on mechanical properties of concrete. *IOP Conference Series: Materials Science and Engineering, 1114, 012008. https://doi.org/10.1088/1757-899X/1114/1/012008*

[26] Mohan, A. B., & Vasudev, R. (2018). Artificial lightweight aggregate through cold bonding pelletization of fly ash: A review. *International Research Journal of Engineering and Technology (IRJET), 5(11), 778–782. https://www.irjet.net/archives/V5/i11/IRJET-V5I11149.pdf*

[27] Ono, K. (2019). A Simple Estimation Method of Weibull Modulus and Verification with Strength Data. *Applied Sciences, 9(8), 1575. https://doi.org/10.3390/app9081575*

[28] Qian, L.-P., Xu, L.-Y., Huang, B.-T., & Dai, J.-G. (2022). Pelletization and properties of artificial lightweight geopolymer aggregates (GPA): One-part vs. two-part geopolymer techniques. *Journal of Cleaner Production, 374, 133933. https://doi.org/10.1016/j.jclepro.2022.133933*

[29] Ke, X., Bernal, S. A., & Provis, J. L. (2016). Controlling the reaction kinetics of sodium carbonate-activated slag cements using calcined layered double hydroxides. *Cement and Concrete Research, 81, 24–37. https://doi.org/10.1016/j.cemconres.2015.11.012*

[30] European Committee for Standardization. (2013). *EN 1097-6: Tests for mechanical and physical properties of aggregates Part 6: Determination of particle density and water absorption (BS EN 1097-6:2013). BSI Standards Ltd.*

[31] British Standards Institution. (2013). BS EN 1097-6:2013 *Tests for mechanical and physical properties of aggregates Part 6: Determination of particle density and water absorption. British Standards Institution.*

[32] Yliniemi, J., Paiva, H., Ferreira, V. M., Tiainen, M., & Illikainen, M. (2017). Development and incorporation of lightweight waste-based geopolymer aggregates in mortar and concrete. *Construction and Building Materials, 131, 784–792. https://doi.org/10.1016/j.conbuildmat.2016.11.017*

[33] Alqahtani, F. K., Rashid, K., Zafar, I., & Khan, M. I. (2021). Assessment of morphological characteristics and physico-mechanical properties of geopolymer green foam lightweight aggregate formulated by microwave irradiation. *Journal of Building Engineering, 35, 102081. https://doi.org/10.1016/j.jobe.2020.102081*

[34] Liu, S., Zhang, W., Xu, M., Wang, F., Hu, Y., & Li, B. (2024). Development of cold-bond artificial aggregate with excavated soil and alkali-activated slag. *Case Studies in Construction Materials, 21, e03451. https://doi.org/10.1016/j.cscm.2024.e03451*

[35] Kursula, K., Perumal, P., Ohenoja, K., & Illikainen, M. (2022). Production of artificial aggregates by granulation and carbonation of recycled concrete fines. *Journal of Materials Cycles and Waste Management, 24, 2141–2150. https://doi.org/10.1007/s10163-022-01457-y*

[36] Dong, B., Chen, C., Wei, G., Fang, G., Wu, K., & Wang, Y. (2022). Fly ash-based artificial aggregates synthesized through alkali-activated cold-bonded pelletization technology. *Construction and Building Materials, 344, 128268. https://doi.org/10.1016/j.conbuildmat.2022.128268*

[37] Tajra, F., Abd Elrahman, M., & Stephan, D. (2019). The production and properties of cold-bonded aggregate and its applications in concrete: A review. *Construction and Building Materials, 225, 29–43. https://doi.org/10.1016/j.conbuildmat.2019.07.219*

[38] Liu, S., Zhang, W., Xu, M., Wang, F., Hu, Y., & Li, B. (2024). Development of cold-bond artificial aggregate with excavated soil and alkali-activated slag. *Case Studies in Construction Materials, 21, e03451. https://doi.org/10.1016/j.cscm.2024.e03451*

[39] Kockal, N. U., & Ozturan, T. (2011). Durability of lightweight concretes with lightweight fly ash aggregates. Construction and Building Materials, 25*(3), 1430–1438. https://doi.org/10.1016/j.conbuildmat.2010.09.022*

[40] Wang, H., Qian, L.-P., Xu, L.-Y., Li, Y., & Guan, H. (2024). Upcycling of waste rubber using pelletized artificial

geopolymer aggregate technology. *Developments in the Built Environment, 20, 100554. https://doi.org/10.1016/j.dibe.2024.100554*

[41] Almadani, M., Razak, R. A., Abdullah, M. M. A. B., & Mohamed, R. (2022). Geopolymer-Based Artificial Aggregates: A Review on Methods of Producing, Properties, and Improving Techniques. *Materials, 15(16), 5516. https://doi.org/10.3390/ma15165516*

[42] Kockal, N. U., & Ozturan, T. (2011). Characteristics of lightweight fly ash aggregates produced with different binders and heat treatments. *Cement and Concrete Composites, 33(1), 61–67. https://doi.org/10.1016/j.cemconcomp.2010.09.007*

[43] Cerný, V., Melichar, J., & Kocianova, M. (2017). Lightweight Aggregate Produced with Cold-Bonding of Fly Ash and Binder. *In Materials Science Forum (Vol. 908, pp. 94–99). Trans Tech Publications, Ltd. https://doi.org/10.4028/www.scientific.net/msf.908.94*

[44] Tian, K., Wang, Y., Hong, S., Zhang, J., Hou, D., Dong, B., & Xing, F. (2021). Alkali-activated artificial aggregates fabricated by red mud and fly ash: Performance and microstructure. *Construction and Building Materials, 281, 122552. https://doi.org/10.1016/j.conbuildmat.2021.122552*

[45] Shivaprasad, K. N., & Das, B. B. (2021). Study on the production factors in the process of production and properties of fly ash-based coarse aggregates. Advances in Civil Engineering, *2021, Article 4309569. https://doi.org/10.1155/2021/4309569*

[46] Jiang, Y., & Ling, T.-C. (2020). Production of artificial aggregates from steel-making slag: Influences of accelerated carbonation during granulation and/or post-curing. *Journal of CO_2 Utilization, 36, 135–144. https://doi.org/10.1016/j.jcou.2019.11.009*

[47] Tuncel, E. Y., & Pekmezci, B. Y. (2018). A sustainable cold bonded lightweight PCM aggregate production: Its effects on concrete properties. *Construction and Building Materials, 181, 199–216. https://doi.org/10.1016/j.conbuildmat.2018.05.269*

[48] Lin, J., Mo, K. H., Goh, Y., & Onn, C. C. (2023). Potential of municipal woody biomass waste ash in the production of cold-bonded lightweight aggregates. *Journal of Building Engineering, 63(Part A), 105392. https://doi.org/10.1016/j.jobe.2022.105392*

[49] Ren, P., Ling, T.-C., & Mo, K. H. (2021). Recent advances in artificial aggregate production. *Journal of Cleaner Production, 291, 125215. https://doi.org/10.1016/j.jclepro.2020.125215*

[50] Tang, P., Xuan, D., Cheng, H. W., Poon, C. S., & Tsang, D. C. W. (2020). Use of CO_2 curing to enhance the properties of cold bonded lightweight aggregates (CBLAs) produced with concrete slurry waste (CSW) and fine incineration bottom ash (IBA). *Journal of Hazardous Materials, 381, 120951. https://doi.org/10.1016/j.jhazmat.2019.120951*